Some Recent Observational Constraints on the Duty Cycle, Magnetization and Energy Dissipation in AGN Jets

Łukasz Stawarz (Jagiellonia University, Kraków)
Epiphany 2022

Large-scale jets and lobes in AGN: why should we care?

Blazars:

- bright & numerous, however
- highly relativistic (bulk Lorentz factors $\Gamma \sim 10 - 100$), so beaming factors $\sim \delta^4$ huge and rather uncertain, also
- unresolved (possible scales range from $r_g \sim 10^{14}\,\mathrm{cm}$ up to $\sim 0.1 - 1\,\mathrm{pc}$), and
- evolving in a photon- and gas-rich circumnuclear environment; finally
- highly variable (from minutes to years and decades), so truly MWL data rarely simultaneous, with poor spectral coverage during flaring states.

Large-scale jets & lobes:

- typically low fluxes/surface brightness, but then
- bulk velocities rather moderate (jet termination shocks only mildly relativistic, lobes' expansion velocities non-relativistic), and
- often resolved at radio, optical, and X-ray (or even HE gamma-ray) photon energies, so the emission region linear scales much better constrained, also
- evolving in a much cleaner ambient medium (ISM/ICM); finally
- steady emitters (at least on month/yearly timescales), so non-simultaneity of the MWL data is less of an issue…

-> all in all, the modeling results are much more robust…

Evolving jets: from young and compact up to old giants

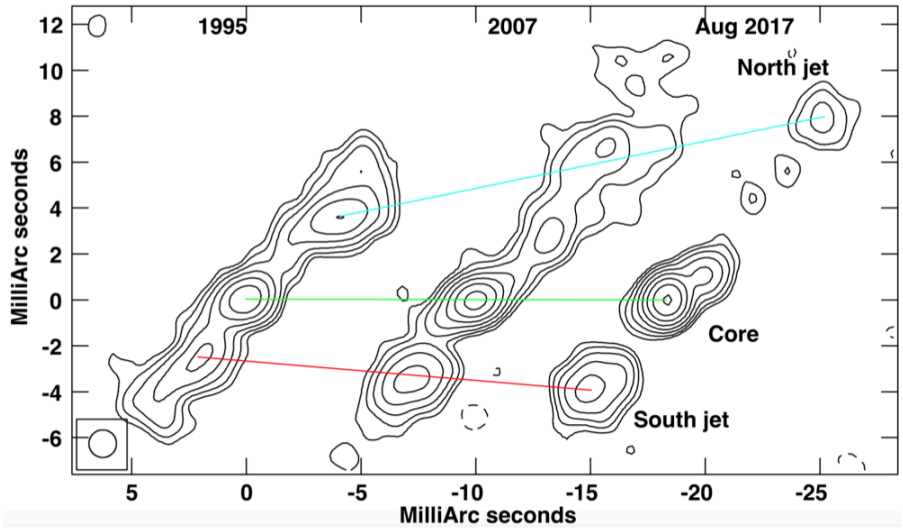

Principe et al. 2020
the youngest confirmed radio galaxy NGC 3894
linear size ~ 2pc, age ~60yrs, expansion velocity ~0.3c, inclination ~ 20deg

Machalski et al. 2008, 2011
the largest radio galaxy identified so far J1420-0545
linear size ~ 4.7 Mpc, age ~100 Myrs, expansion velocity ~0.1c

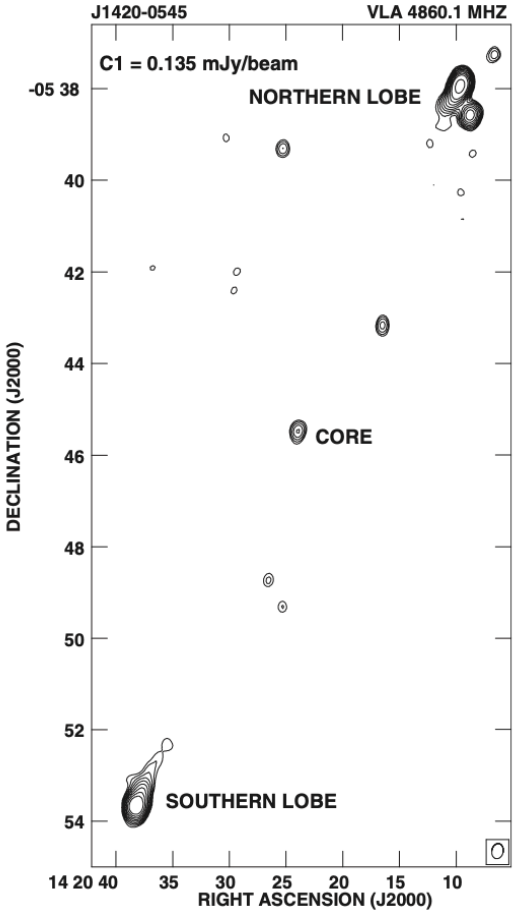

Intermittent jet activity

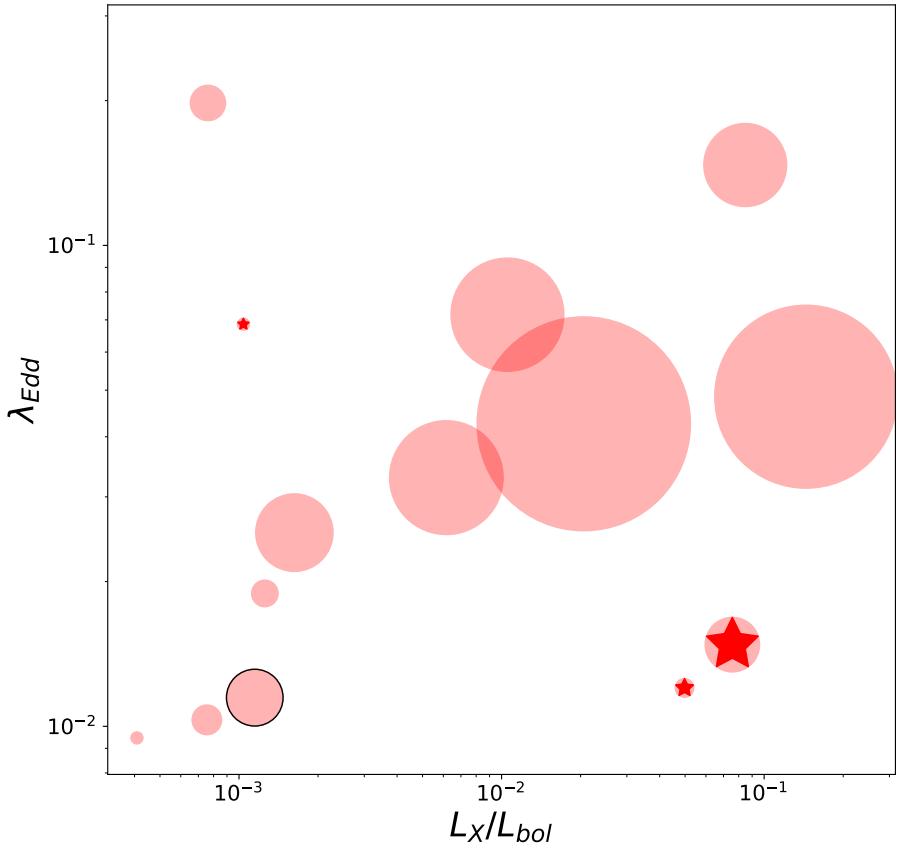

Wójtowicz, LS, et al. 2020:

Dependence of the jet production efficiency on the combination of the disk accretion rate $\lambda_{\rm Edd} \equiv L_{\rm bol}/L_{\rm Edd}$ and the corona "hardness" ratio $L_{\rm X}/L_{\rm bol}$, for the sample of the youngest radio galaxies; the jet power is coded by the size of the symbols, and expressed in units of mass accretion rate $\eta_{\rm j} \equiv L_{\rm j}/\dot{M}_{\rm acc}c^2$. Compton-thick sources are marked by red stars.

…the dependence which is well established for XRBs (see A. Zdziarski's talk)

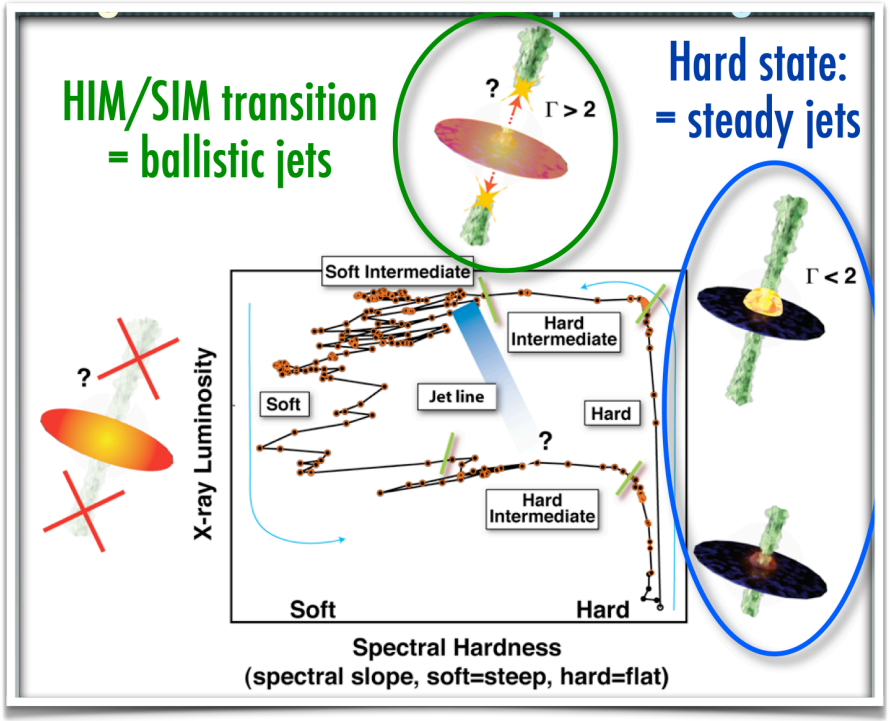

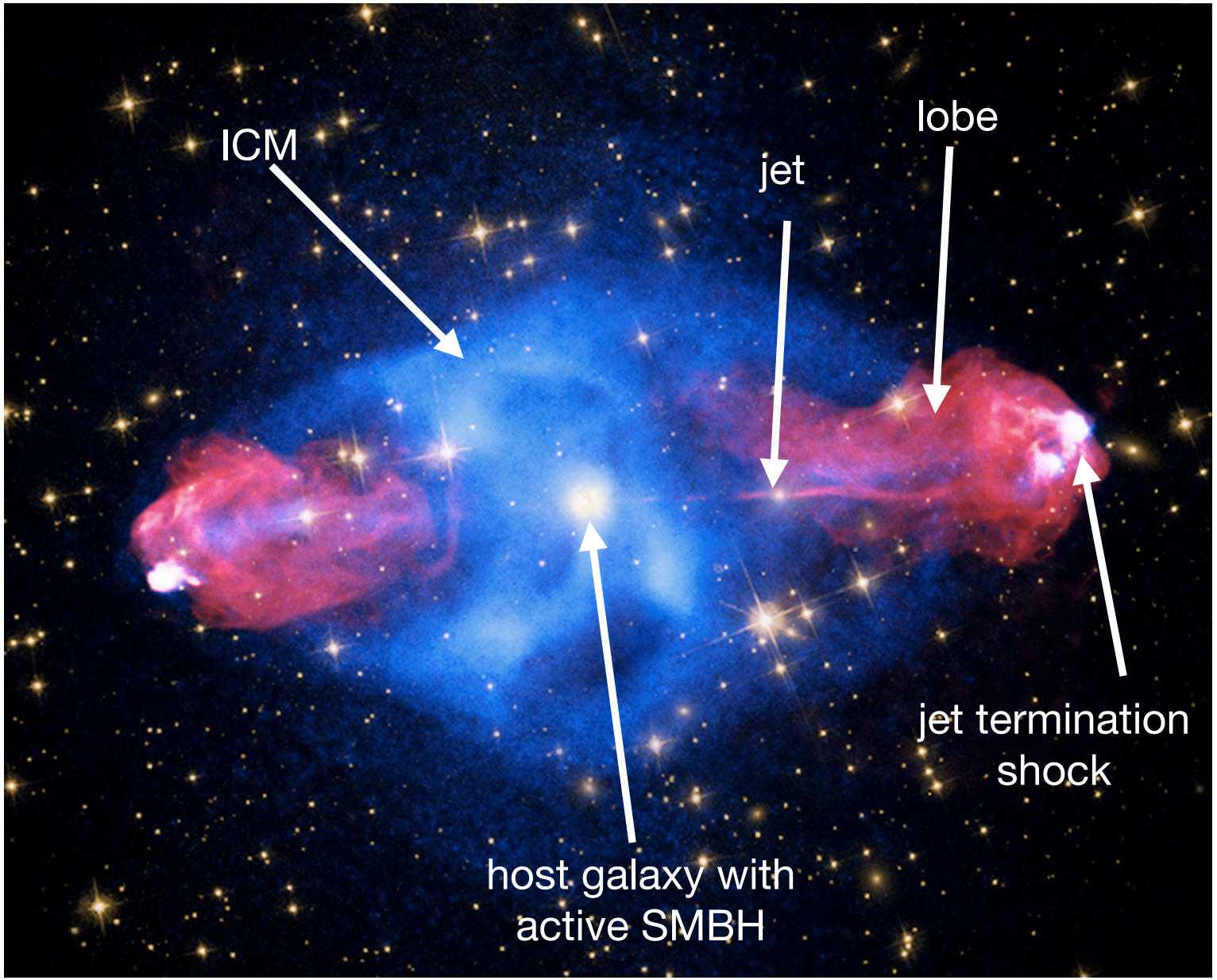

Lobes' evolution

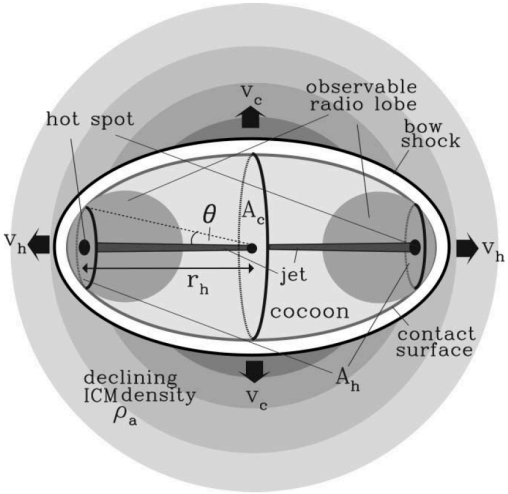

The overall dynamical evolution of hot overpressure cocoons inflated by light relativistic jets, is well understood (Begelman & Cioffi, Kaiser & Alexander, Kino & Kawakatu)

Large-scale jets in X-rays

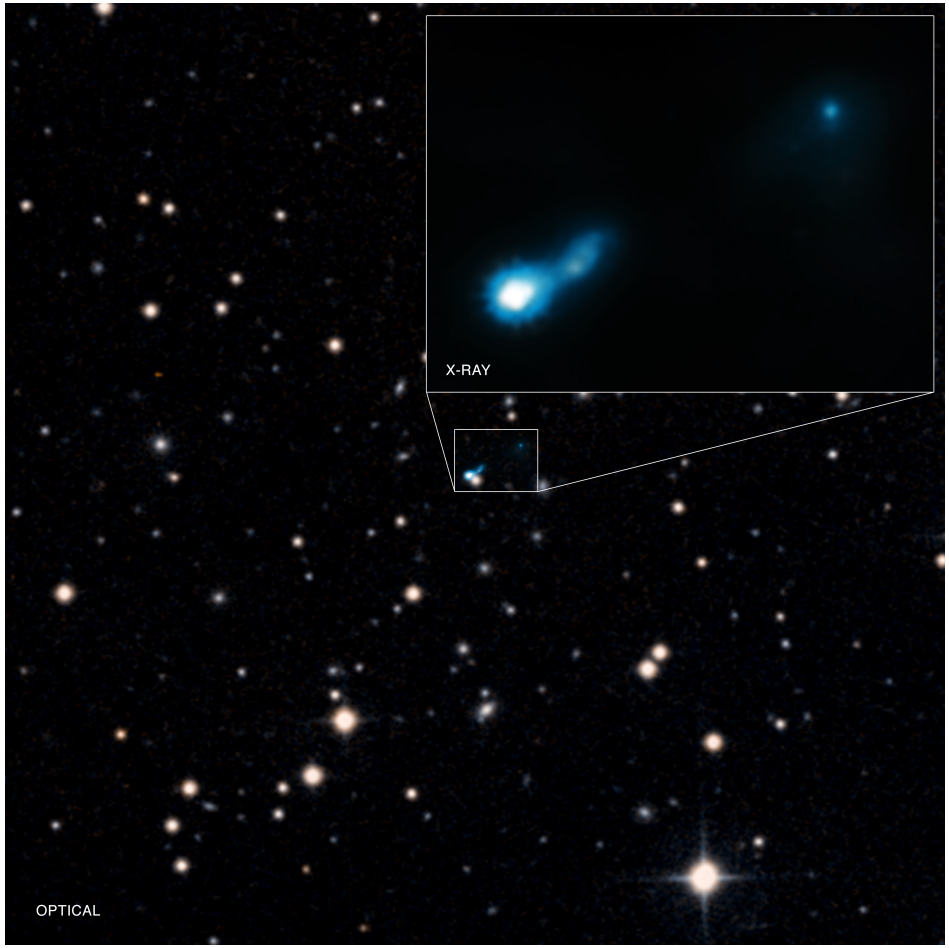

Simionescu, LS, et al. 2016:
B3 0727+409, a luminous quasar at z = 2.5, with the X-ray jet resolved with Chandra ~ 300 kpc projected!

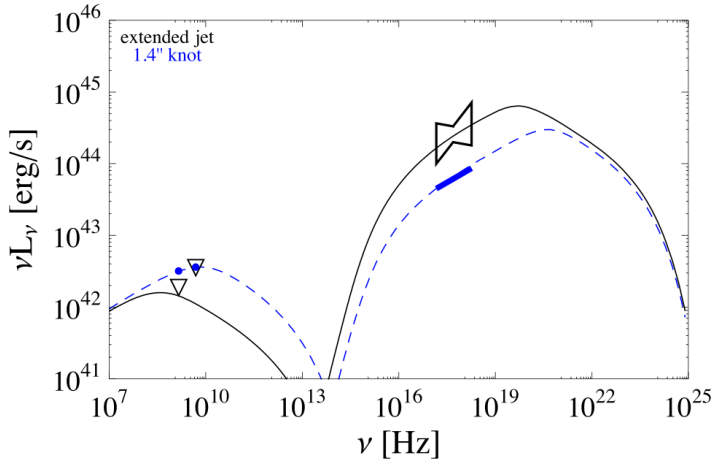

If the observed X-ray emission is due to inverse-Comptonization of the CMB photons (Tavecchio et al. 2000), large-scale jets appears highly relativistic up to kpc/Mpc distances ($\Gamma \sim 10$), and particle-dominated ($\sigma \ll 1$), with no significant energy dissipation from the jet launching regions (blazar scales) up to terminal regions.

Large-scale jets in X-rays

$$u_{\rm cmb} \propto (1+z)^4$$

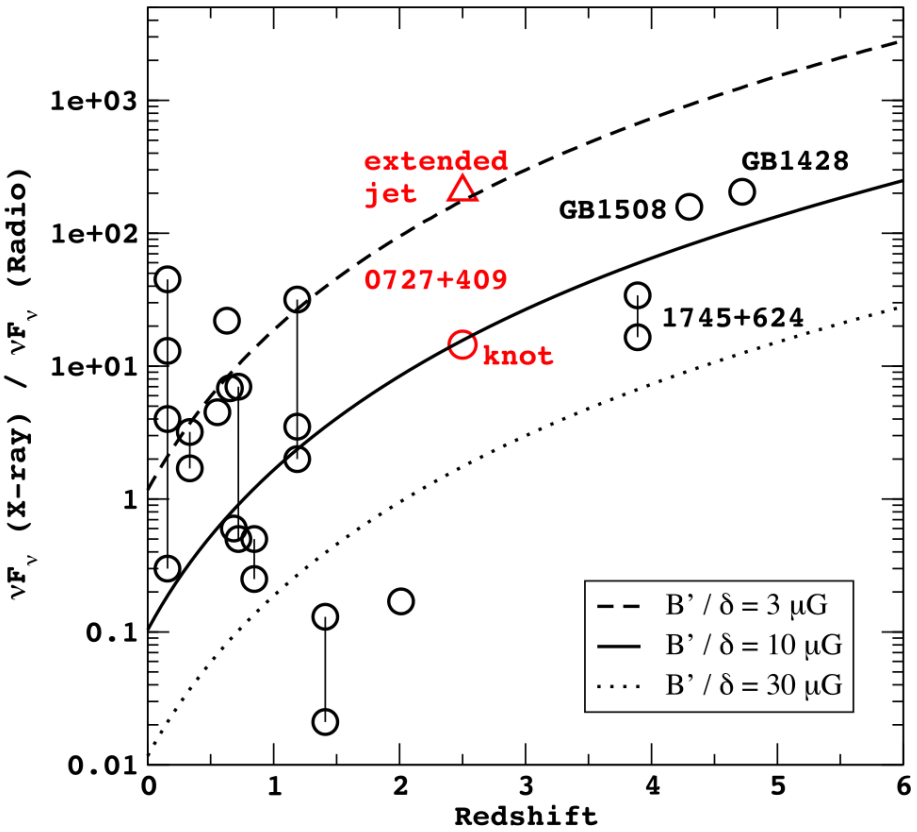

Alternatively, the X-ray emission of large-scale jets may be synchrotron in origin (LS & Ostrowski 2002) — this would imply very efficient electron acceleration ($\gamma_{\rm max} \sim 10^8$) and allow for a higher magnetization of the jet plasma on large-scales ($\sigma \geq 1$).

Acceleration sites often discussed in this context:
shear boundary layers
(Ostrowski, Rieger & Duffy, Wang & Reville)

Large-scale jets: particle- or magnetic-dominated?

Król, LS, et al. 2022 (to be submitted)

A simple analytical model for relativistic current-carrying jets at larger distances from their launching sites, assuming a cylindrical axi-symmetric geometry with a radial velocity shear, purely toroidal configuration for the jet magnetic field, and ultra-relativistic equation of state for the jet particles.

As long as the jet plasma is in **magnetohydrostatic equilibrium** $\vec{\nabla} P = \vec{J} \times \vec{B}$, and pressure radial profiles are continuous, such outflows have to be always particle dominated, in the sense that the ratio of the electromagnetic to particle energy fluxes integrated over the jet cross-section area, tends to be below unity, i.e. the jet magnetization parameter $\sigma < 1$.
At the same time, for particular magnetic and radial velocity profiles, magnetic pressure may still dominate over particle pressure for certain ranges of the jet radius, i.e. that the local jet plasma parameter $\beta_{\rm pl}^{-1} > 1$.

Jet may be globally magnetically dominated ($\sigma \gtrsim 1$) only in the case of huge pressure jumps/discontinuities at certain jet radii (by several orders of magnitude), and negligible velocity shear (essentially, a completely non-magnetised jet spine surrounded by a force-free boundary layer).

$$\partial_r P = -\frac{1}{8\pi r^2}\,\partial_r\left(\frac{r^2 B_\phi^2}{\Gamma^2}\right)$$

$$\sigma \equiv \frac{L_B}{L_p} = \frac{1}{16\pi}\,\frac{\int dr\, r\, \beta\, B_\phi^2}{\int dr\, r\, \beta\, \Gamma^2\, P}$$

Termination shocks: case study of Pictor A

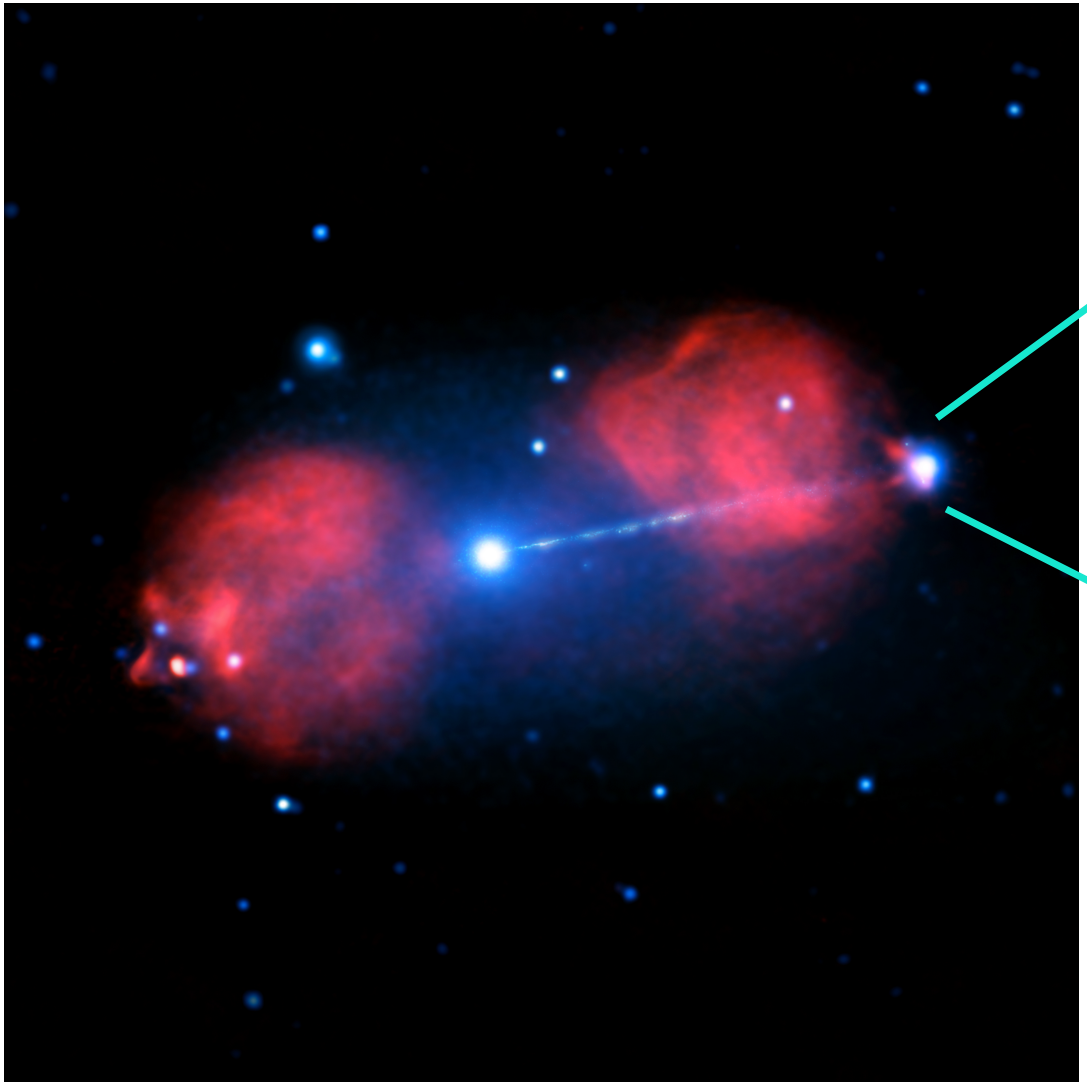

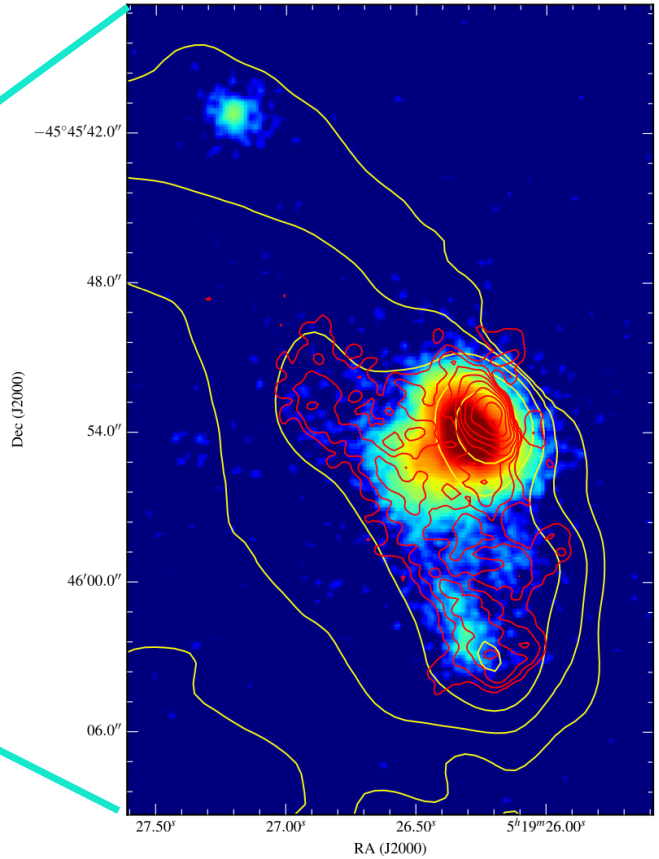

Hardcastle et al. 2016:
deep Chandra observations (~0.5 Ms)
of the radio galaxy Pictor A

Termination shocks: case study of Pictor A

Thimmappa, LS, et al. 2020:
re-analysis of the Chandra data
& image deconvolution

Table 1
Observational Data and Spectral Fitting Results

ObsID	Date	MJD	Exposure (ks)	θ (arcmin)	Γ	red.χ^2	$F_{0.5-7.0\,\mathrm{keV}}$ (10^{-13} erg cm^{-2} s^{-1})	Counts[a]
346	2000-01-18	51561	25.8	3.50	2.01 ± 0.05	0.272	5.41 (+0.20/−0.45)	3461
3090	2002-09-17	52534	46.4	0.11	1.96 ± 0.03	0.377	5.64 (+0.03/−0.20)	5278
4369	2002-09-22	52539	49.1	0.11	1.99 ± 0.03	0.426	5.61 (+0.11/−0.15)	5564
12039	2009-12-07	55172	23.7	3.35	1.98 ± 0.06	0.260	5.71 (+0.02/−0.10)	2290
12040	2009-12-09	55174	17.3	3.35	2.07 ± 0.08	0.265	5.47 (+0.08/−0.25)	1710
11586	2009-12-12	55177	14.3	3.35	2.11 ± 0.09	0.212	5.39 (+0.21/−0.40)	1427
14357	2012-06-17	56095	49.3	3.07	2.05 ± 0.05	0.321	5.88 (+0.06/−0.14)	3043
14221	2012-11-06	56237	37.5	3.10	2.08 ± 0.05	0.356	5.84 (+0.01/−0.11)	3248
15580	2012-11-08	56239	10.5	3.10	2.08 ± 0.14	0.235	5.24 (+0.30/−0.21)	935
14222	2014-01-17	56674	45.4	3.30	2.00 ± 0.05	0.329	5.78 (+0.12/−0.10)	3428
16478	2015-01-09	57031	26.8	3.32	1.95 ± 0.08	0.232	5.30 (+0.15/−0.54)	1657
17574	2015-01-10	57032	18.6	3.32	2.04 ± 0.11	0.209	5.33 (+0.26/−0.21)	1187

Note.
[a] Total number of counts within the 0.5–7.0 keV range from a circular region with a radius 20 px centered on the hotspot.

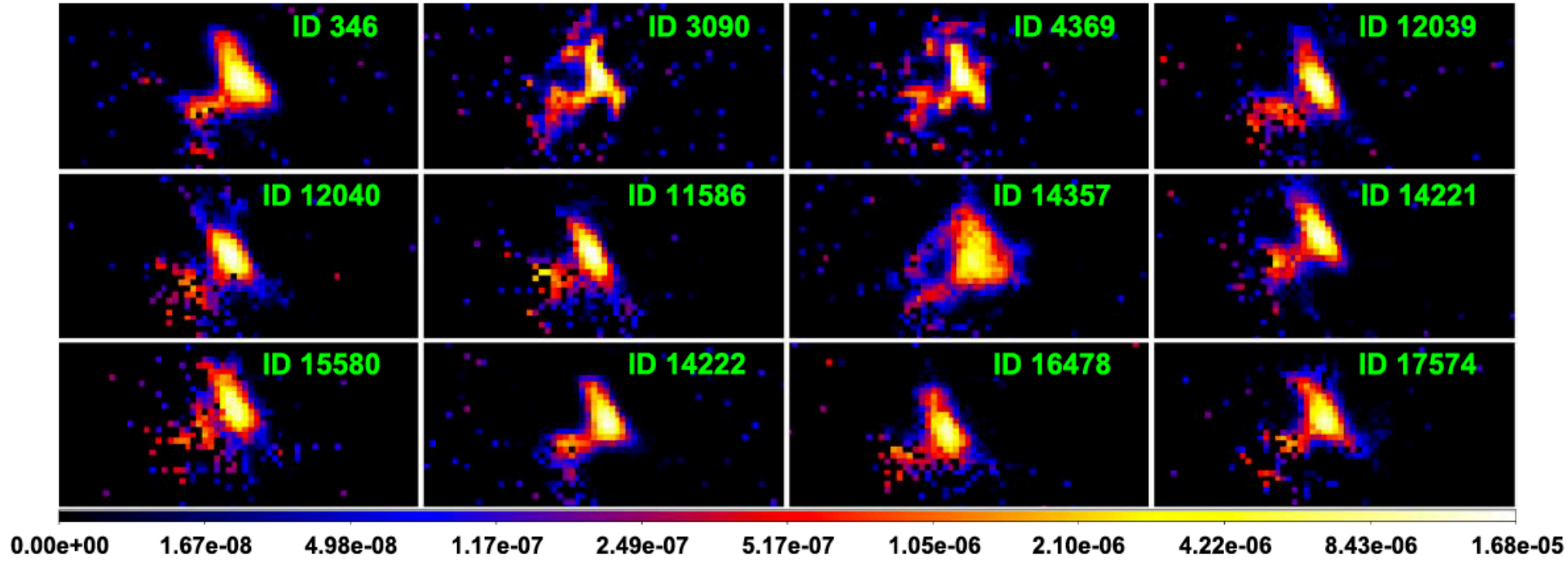

Figure 6. Deconvolved Chandra images of the W hotspot in Pictor A at 0.5 px resolution. Each image results from averaging over the restored images for 100 PSF realizations using the LRDA on the exposure-corrected maps. The color scale gives the count rate (cts s^{-1}).

Termination shocks: case study of Pictor A

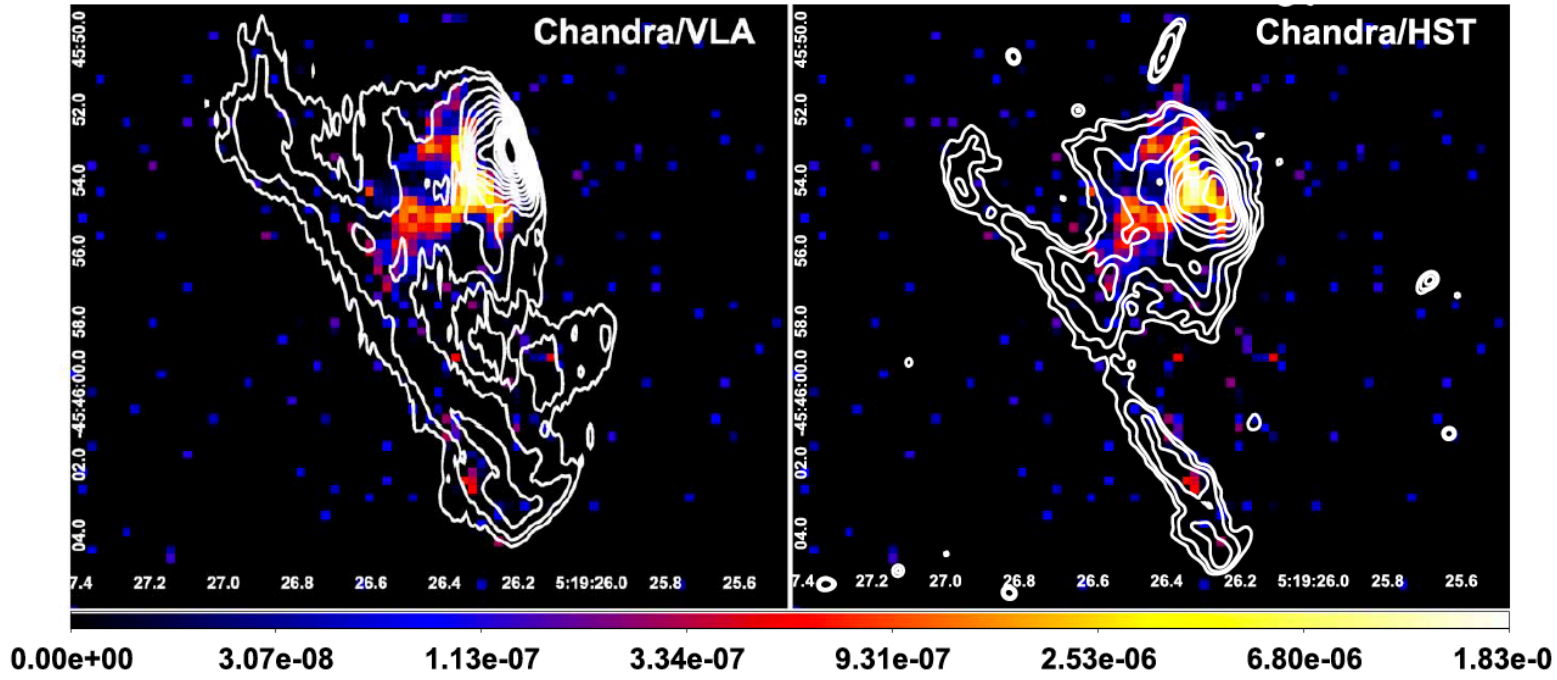

Figure 7. Deconvolved exposure-corrected Chandra image of the W hotspot in Pictor A at 0.5 px resolution for the ObsID 3090, averaged over 100 random realizations of the PSF, with the radio (3.6 cm wavelength, beam size $0\farcs77 \times 0\farcs17$, position angle $-0\fdg4$) VLA contours superimposed (left panel) and optical F606W filter (5918 Å, 90% encircled energy within radius $0\farcs35$) Hubble Space Telescope ACS/WFC contours superimposed (right panel). Radio contours are spaced with a factor of $\sqrt{2}$ between 0.552% and 70.71% of the peak intensity of 215 mJy beam^{-1}. Optical contours are spaced with a factor of $\sqrt{2}$ between 0.008 and 3 cts s^{-1}.

Thimmappa, LS, et al. 2020:

we were able to resolve the X-ray structure of the hotspot into (i) the jet-like feature located in between the radio/optical filament and the termination shock, and (ii) the disk-like or conical feature perpendicular to the jet axis, and located ~1 kpc upstream the intensity peak of the radio hotspot. We believe that this later feature — resolved in its longitudinal direction to be ~3 kpc long, while remaining basically unresolved in its transverse direction, with the corresponding scale upper limit of < 200 pc — marks the position of the reverse shock front in the system, where efficient particle acceleration takes place.

Particle acceleration at termination shocks

Wójtowicz, LS, et al. 2021:
In the sample of 270 radio galaxies subjected to detailed dynamical-radiative modeling, we notice a significant and nonobvious correlation between the spectral index of the nonthermal radio emission continuum (rest-frame frequencies 0.4 and 5 GHz) — and hence the particle injection index at the jet termination shock — and density of the ambient medium.

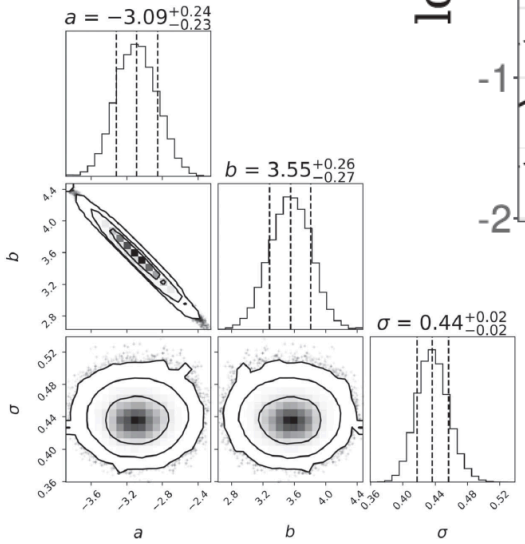

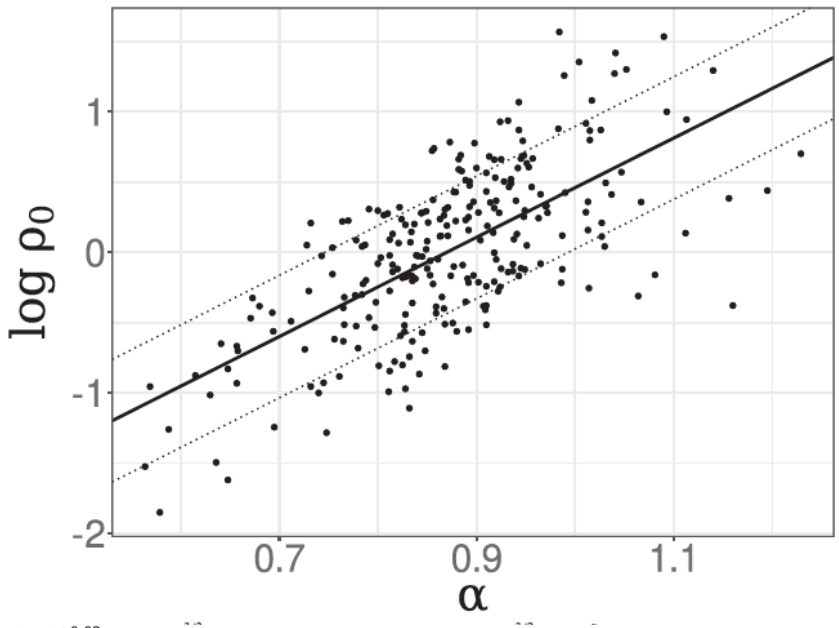

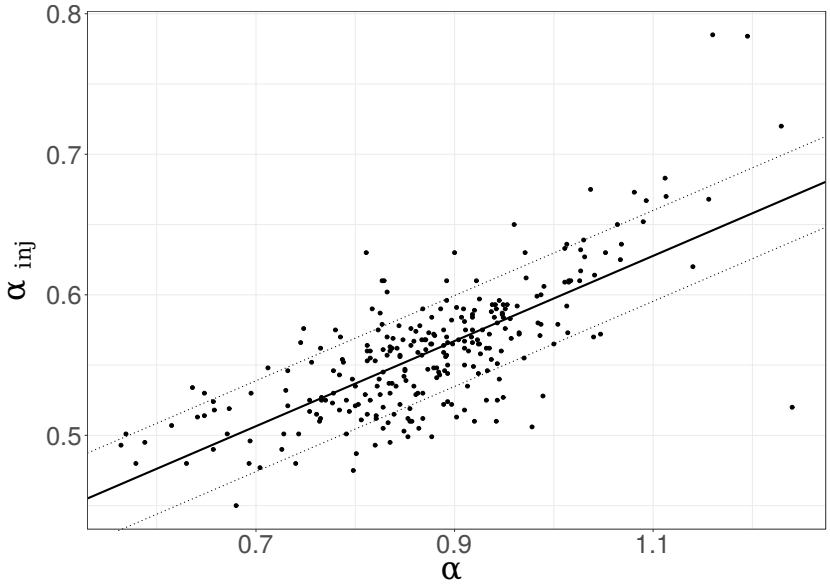

-> the increasing density of the ambient medium seems to decrease the efficiency of accelerating jet electrons at the termination shocks to ultrarelativistic energies

Extended lobes: case study of Pictor A

Thimmappa, LS, et al. 2021:

Complex internal structure of the extended lobes in Pictor A: highly polarized radio filaments/domains, X-ray shells/ enhancements.

Low-polarization regions associated with the magnetic field's line-of-sight reversals most likely due to a thermal matter with mass $\mathcal{O}(10^9 M_\odot)$, distributed within thin shells or filaments (see Anderson et al. 2018).

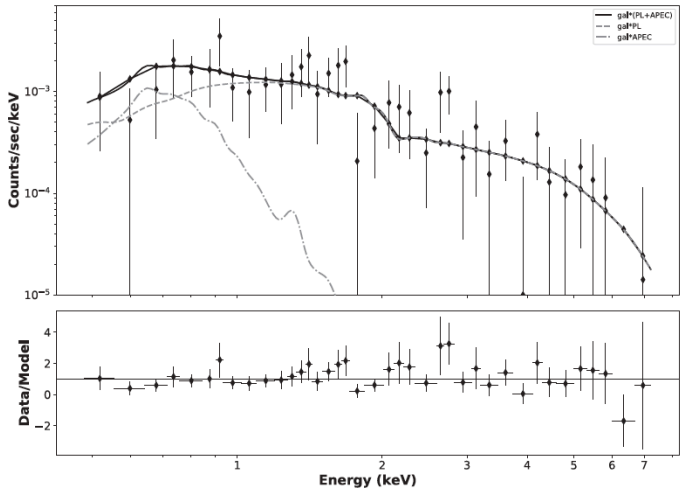

Power-law +APEC	Photon index Γ	$1.27^{+0.27}_{-0.41}$
	PL normalization	$3.12^{+0.78}_{-0.92} \times 10^{-6}$
	Temperature kT	$0.27^{+0.14}_{-0.07}$
	APEC normalization	$5.04^{+4.54}_{-2.63} \times 10^{-6}$
	Background photon index Γ_{bck}	$0.27^{+0.08}_{-0.08}$
	Background normalization	$6.52^{+0.61}_{-0.56} \times 10^{-6}$

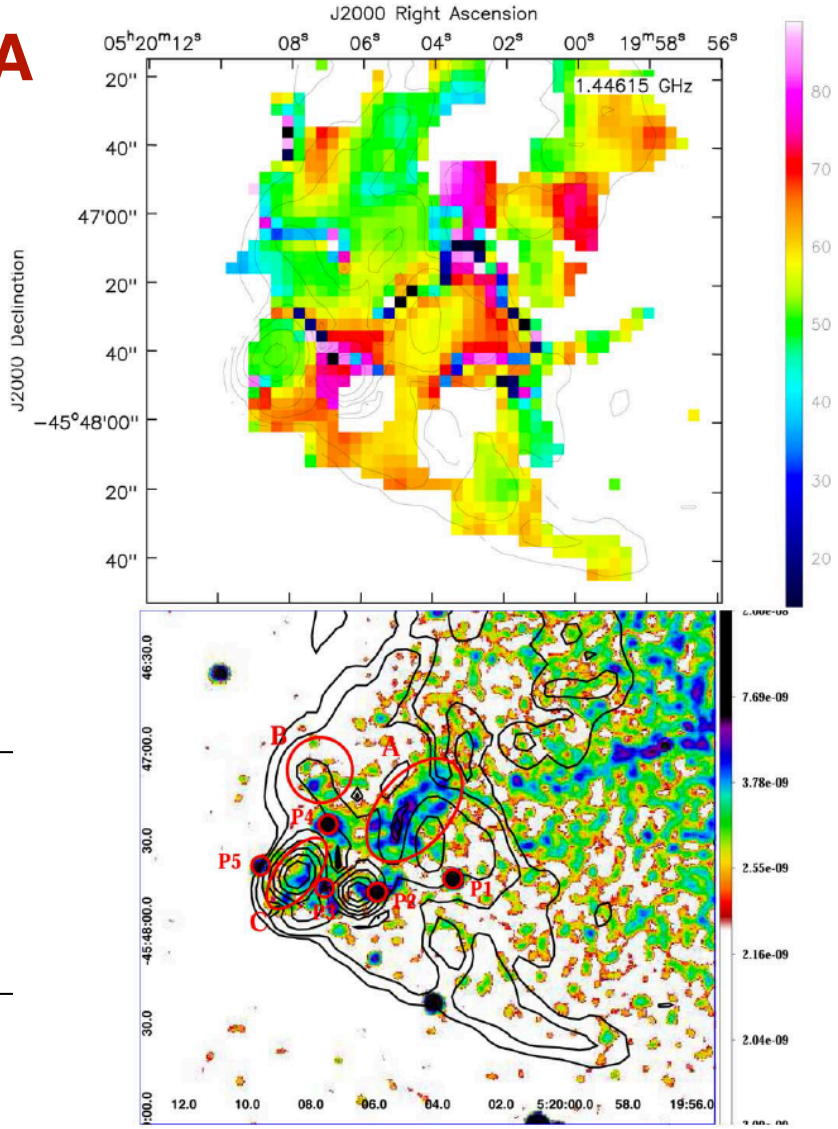

Figure 3. Top: A zoomed-in view of the RM distribution within the E hotspot region in Pictor A, with the polarized intensity *L*-band contours superimposed, at a 10″ resolution. Contours start from the 3σ confidence level and are scaled by $\sqrt{2}$. Bottom: A zoomed-in view of the 0.5–7.0 keV emission of the E hotspot region in Pictor A, with the 1.45 GHz polarized intensity contours (black) superimposed. The 0.5–7.0 keV Chandra image is smoothed with a 3σ Gaussian (radius 5 px). Radio contours start from the 3σ confidence level. Regions selected for the Chandra data analysis are labeled and indicated by red contours.

Extended lobes: case study of Pictor A

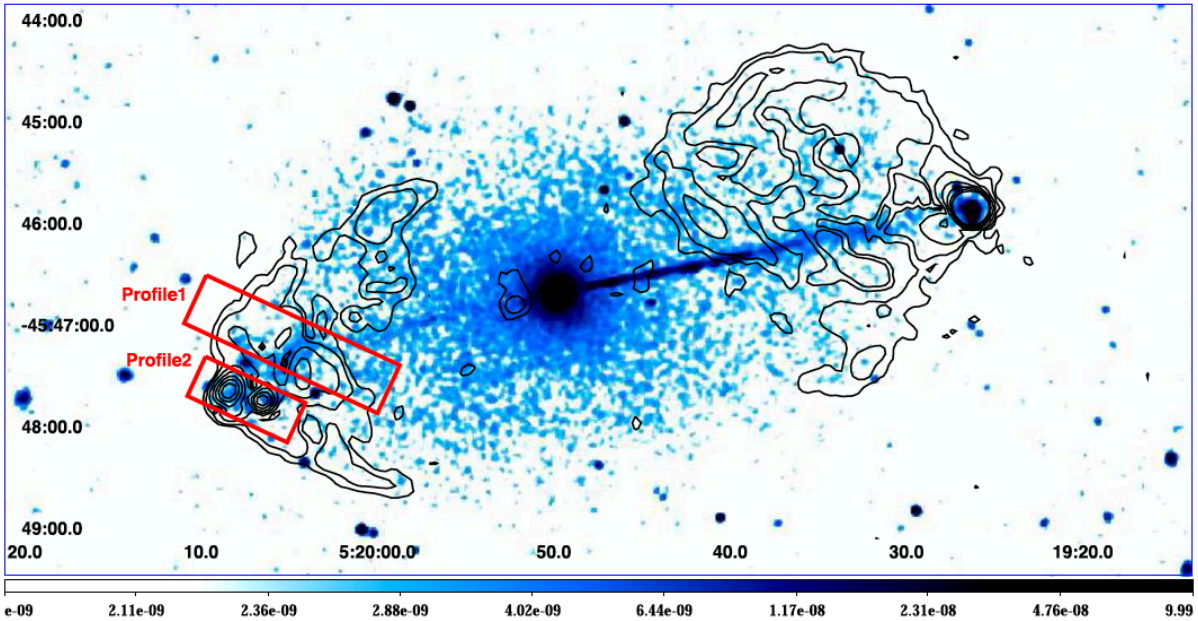

Figure 6. The exposure-corrected 0.5–7.0 keV merged Chandra image of the entire structure of Pictor A, smoothed with a 3σ Gaussian radius, with the 1.45 GHz VLA polarized intensity (3σ) contours superimposed. The two elongated red rectangles denote the areas across the high-polarization regions of the E lobe, for which we extracted the surface brightness profiles at X-ray and radio frequencies.

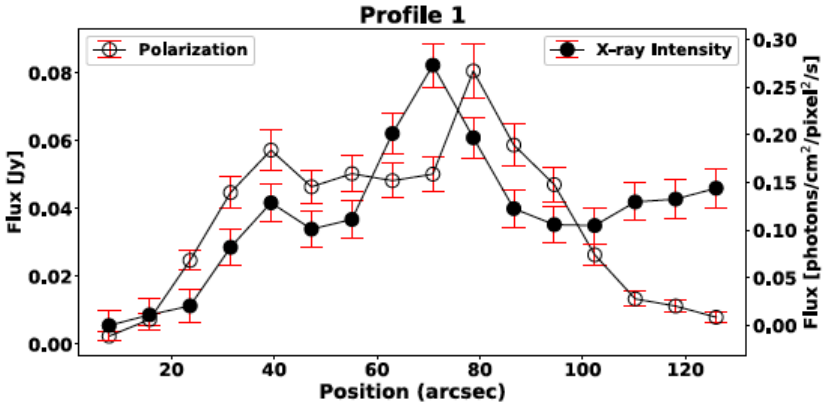

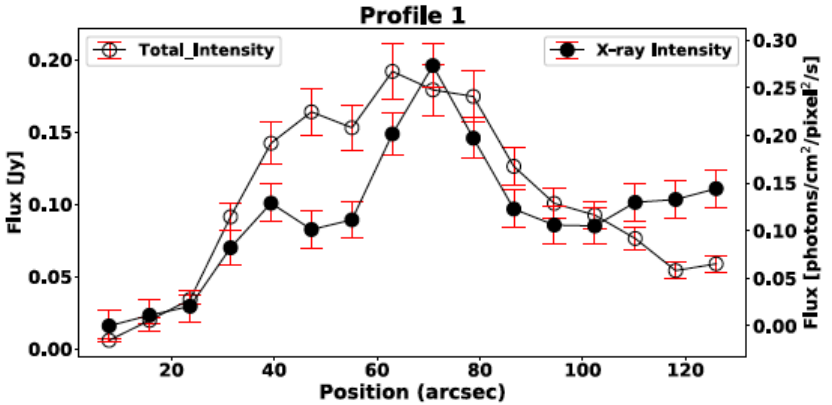

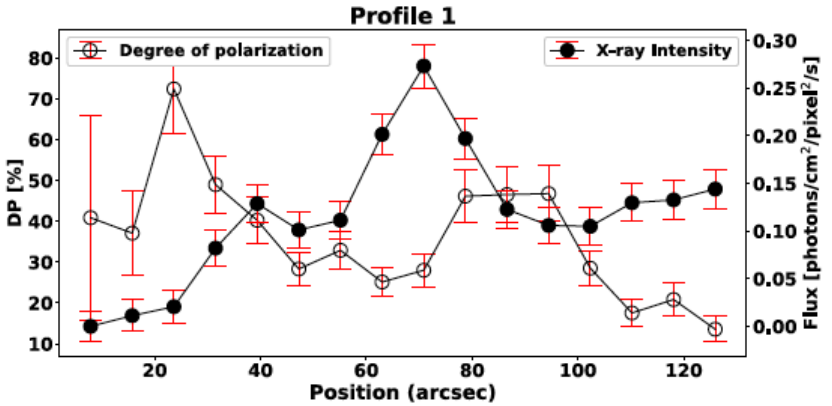

Thimmappa, LS, et al. 2021:

The total pressure of the thermal gas within the filament, ~1e-12 dyn/cm2, comparable to that of the lobes' magnetic field for the magnetic field intensity B ~ 6 μG, which is, in fact, very close to the equipartition value, i.e., the value obtained by assuming pressure balance between ultrarelativistic radio-emitting electrons and the lobes' magnetic field.

Giant Lobes of Centaurus A

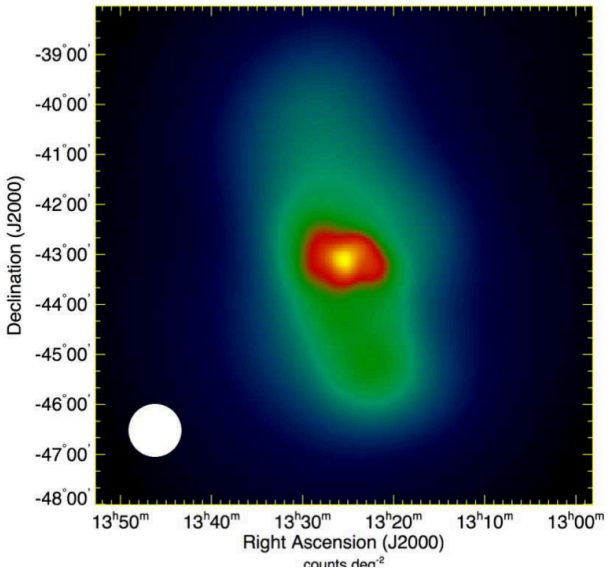

Abdo et al. 2010:

Fermi-LAT detection of the giant lobes in Cen A at HE gamma-rays, implies that the lobes' non-thermal electrons are in a pressure equilibrium with the lobes' magnetic field ("volume-averaged pressures")

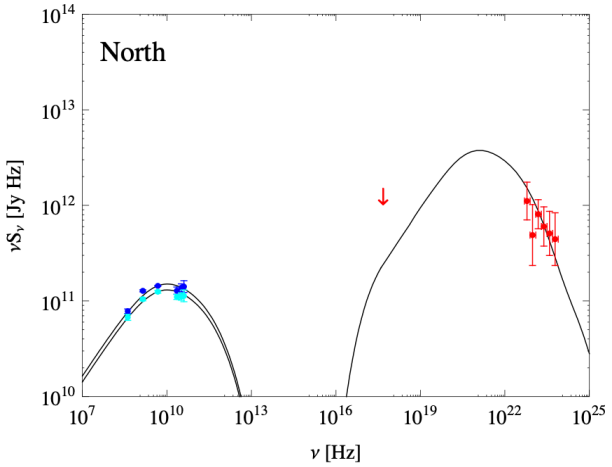

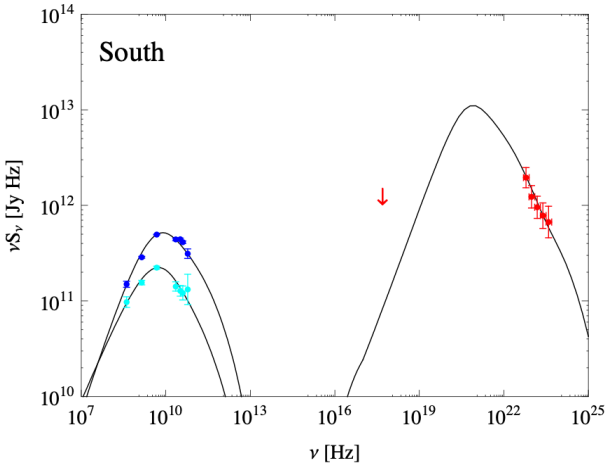

McKinley et al. 2021:

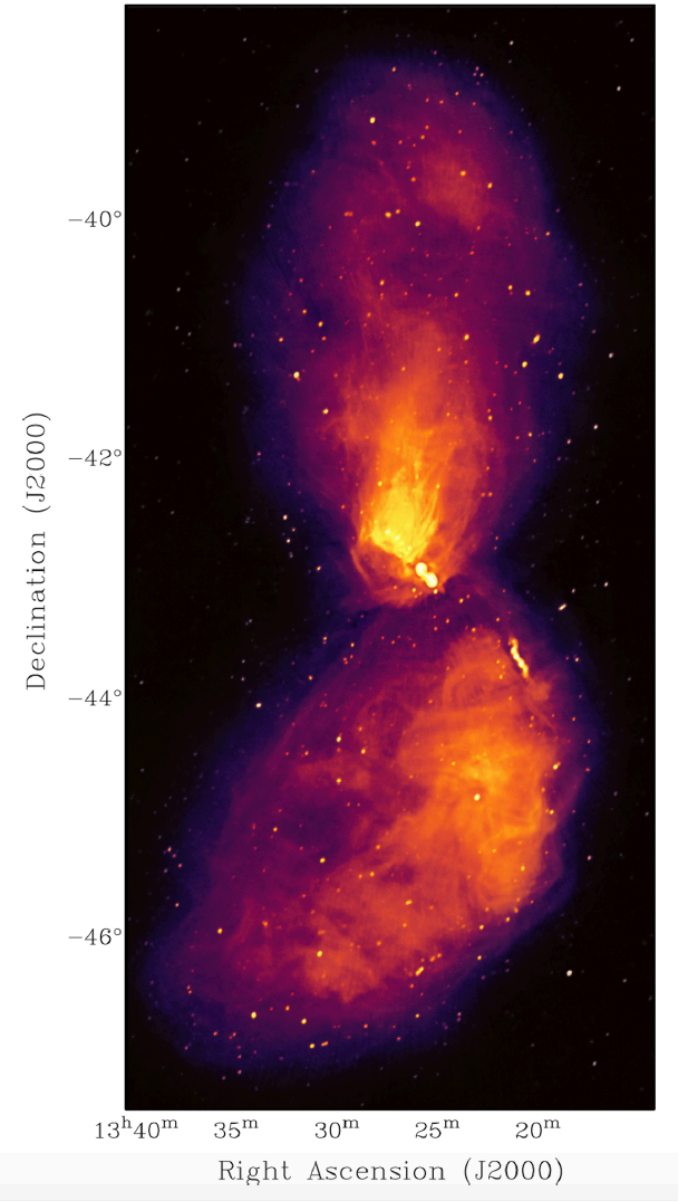

Giant Lobes of Centaurus A

LS et al. 2013:

Suzaku X-ray observations of selected regions within the southern giant lobe of the radio galaxy Centaurus A:

A tentative detection of a soft excess component best fitted by a thermal model with a temperature of kT ~ 0.5 keV, and consistent with a thermal gas filling the bulk of the volume of the lobe and mixed with the non-thermal plasma.

The corresponding pressure appears to be in almost exact equipartition with the volume-averaged non-thermal pressure provided by the radio-emitting electrons and the lobes' magnetic field.

Modeling Results for the Excess Diffuse Emission

$Z/Z_\odot$ (1)	kT (2)	Norm (3)	$F^{abs}_{0.5-2\,keV}$ (4)	Red. χ^2/dof (5)
Lobe 1				
1.0^f	$0.46^{+0.08}_{-0.11}$	$3.11^{+1.11}_{-0.53}$	5.84	1.20/444
0.3^f	$0.45^{+0.08}_{-0.10}$	$9.76^{+3.80}_{-1.88}$	6.12	1.20/444
0.1^f	$0.39^{+0.09}_{-0.07}$	$27.3^{+10.4}_{-7.2}$	6.72	1.20/444
Lobe 2				
1.0^f	$0.64^{+0.05}_{-0.05}$	$2.91^{+0.34}_{-0.35}$	5.83	1.13/515
0.3^f	$0.64^{+0.05}_{-0.05}$	$8.59^{+1.03}_{-1.03}$	6.20	1.13/515
0.1^f	$0.62^{+0.06}_{-0.06}$	$19.1^{+2.61}_{-2.49}$	6.72	1.13/515

Notes. (1) The assumed abundance Z; (2) temperature of the additional thermal component in keV units; (3) the MEKAL normalization of the additional thermal component $\times 10^{-4}$; (4) absorbed 0.5–2 keV flux in units of 10^{-13} erg cm^{-2} s^{-1}/ 0.35 deg^2; (5) reduced χ^2 value/degree of freedom.

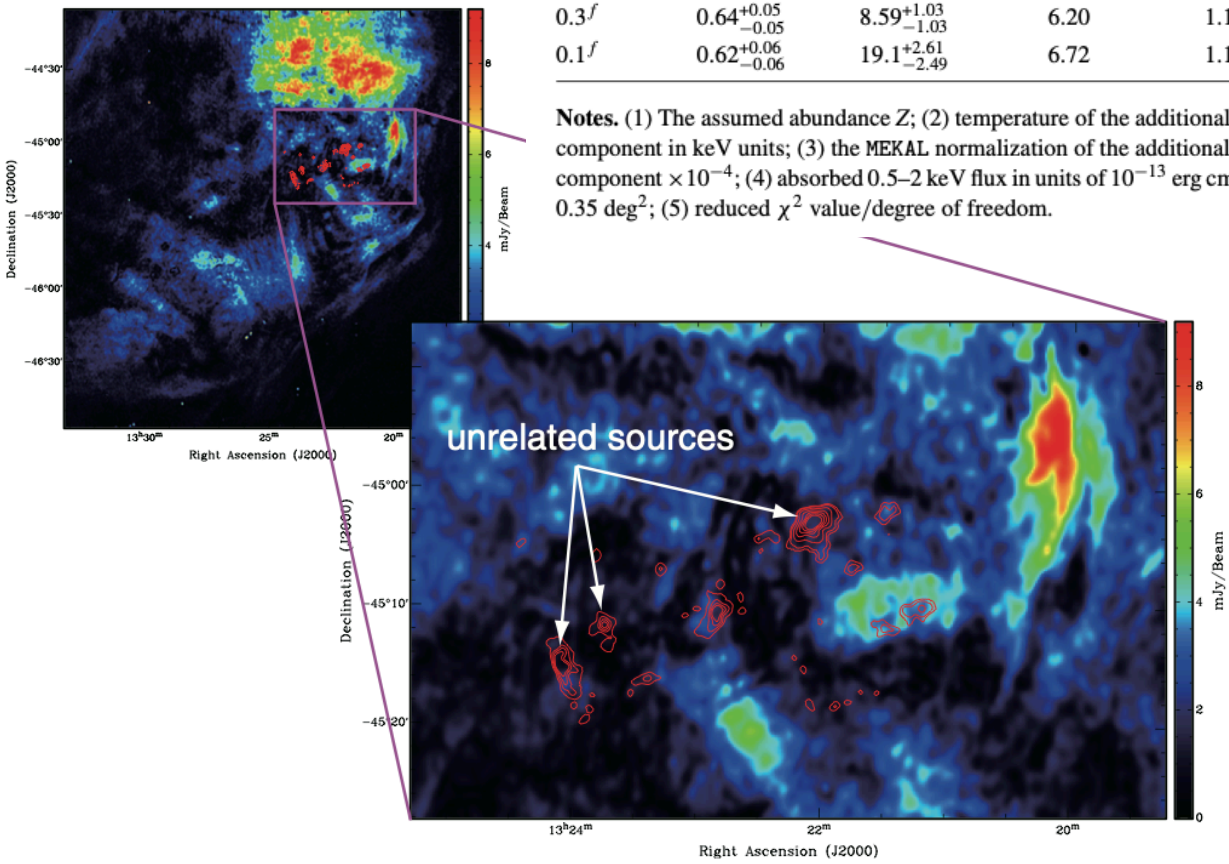

Summary:

Large-scale jets, their termination shocks, and extended lobes in AGN: excellent laboratories of relativistic astrophysical plasma and particle acceleration. Intermittent, evolving structures, depositing huge amounts of power (in a form of a bulk kinetic energy of the jet particles and the electromagnetic flux) directly into the surrounding ISM/ICM

- AGN jets at large scales seems most likely particle dominated, in the sense that the ratio of the electromagnetic to particle energy fluxes integrated over the jet cross-section area, tends to be below unity, i.e. the jet magnetization parameter $\sigma < 1$. At the same time, for particular magnetic and radial velocity profiles, magnetic pressure may still dominate over particle pressure for certain ranges of the jet radius, i.e. that the local jet plasma parameter $\beta_{\rm pl}^{-1} > 1$

- Jet termination regions are the best-studied examples of mildly-relativistic quasi-perpendicular shocks; there we see an efficient electron accelerate up to rather high energies $\gamma_{\rm max} > 10^6$ (in prep.: observational evidence the acceleration takes place at the shock front rather than in the downstream); however, spectral index positively correlated with the environment density — the increasing density of the ambient medium seems to decrease the efficiency of accelerating jet electrons.

- Extended lobes: equipartition between volume-averaged pressures of non-thermal electrons, magnetic field, and partly mixed-in thermal gas; however, a close inspection reveals highly inhomogeneous and non-uniform structure, with radio and X-ray filaments/shells/domains, suggesting significant spatial and temporal variations in the plasma beta parameter around the volume-averaged equilibrium condition $\beta_{\rm pl} \sim 1$.